Commensurate-incommensurate transitions in magnetic bubble arrays with periodic line pinning

Junmin Hu and R. M. Westervelt
Division of Engineering and Applied Sciences and Department of Physics, Harvard University, Cambridge, Massachusetts 02138
(Received 10 June 1996)

We report direct observations of commensurate-incommensurate phase transitions as a function of bubble concentration in a two-dimensional magnetic bubble array subject to periodic line pinning. The pinning lines consist of lithographically produced parallel permalloy bars. Temperature is simulated by an ac magnetic field. The structure function shows a smooth migration of Bragg peaks with density indicating a second order (or weakly first order) commensurate-incommensurate-commensurate transition as the local orientation of the array rotates continuously. We have also identified a commensurate smectic phase. [S0163-1829(97)01801-8]

I. INTRODUCTION

Many experimental systems demonstrate commensurate and incommensurate phases. Typical examples are rare-gas atoms absorbed on graphite,[1,2] thickness modulated superconducting films,[3,4] and layered superconductors.[5,6] When the density of such a system changes, the system commonly undergoes phase transitions between the commensurate and incommensurate phases controlled by the relative strengths of pinning and interaction. It is of considerable theoretical and experimental interest to understand how the commensurate-incommensurate transitions take place in an experimental system. Direct microscopic observation is often difficult, as in experimental studies carried out by x-ray scattering[2] or transport measurements,[4] because of limitations in available imaging techniques. In the magnetic bubble system with artificial pinning,[7] the magnetic bubbles can be visualized by means of the Faraday effect and the pinning lines are visible for the regime we studied. It is our hope that direct observation and understanding of the commensurate-incommensurate phase transitions in the magnetic bubble system will act as a bridge between theoretical prediction and experimental results and provide detailed microscopic picture for future theoretical work.

In this paper we present microscopic observations of the commensurate-incommensurate phase transitions in a two-dimensional magnetic bubble array subject to periodic line pinning. At high bubble concentration a commensurate phase exists with two rows of bubbles per pinning line and hexagonal rotational symmetry. We call this a dislocated triangular array because it has quasi-long-range orientational order but short range positional order due to the action of the disordered substrate potential; such systems are often referred to as hexatics.[8–10] As the concentration decreases, internal stresses are created in the array and force the orientation of the triangular lattice to rotate locally, leading to an incommensurate polycrystalline phase. Upon continuing decrease of the concentration, the array first forms a commensurate smectic phase, which is ordered in the pinning direction but disordered in the perpendicular direction, then forms a new commensurate dislocated triangular array with approximately twice the bubble spacing of the previous triangular array, and finally forms a modulated liquid phase. The structure functions of these new commensurate phases display exactly twice as many sharp Bragg peaks in the perpendicular direction as that of the first commensurate phase. These phase transitions happen by a smooth migration of diffuse Bragg peaks from the first commensurate phase to the subsequent commensurate phases, as for krypton on graphite and layered superconductor theory.[1,5]

II. EXPERIMENTAL METHOD

The ability to introduce artificial pinning into the magnetic bubble array enables us to study the effect of pinning of virtually any strength and geometry on a two-dimensional system. Figure 1(a) schematically illustrates a cross section of the sample. Magnetic bubbles are cylindrical domains of reversed magnetization in a uniaxial ferrimagnetic garnet film, as indicated in Fig. 1(a). Pinning is provided by a thin permalloy film (Ni-Fe 80:20), indicated in Fig. 1(a) by the dark stripes. It is patterned on the film surface using photolithography and electron beam evaporation techniques.[7] The permalloy overlay pins magnetic bubbles underneath by providing flux closure between bubbles and neighboring domains with opposite magnetization. As shown schematically in Fig. 1(a), the pinning geometry is an array of parallel lines with period $s=20$ μm. Each line is 6 μm wide and 51 Å thick. These pinning lines cover the bubble array over an area 1×1 cm^2. The pinning strength is moderate for these parameters: bubbles escape from pinning sites during annealing at incommensurate bubble concentrations.

The force between bubbles is approximately a magnetic dipole-dipole interaction. Two types of pinning occur in this system: moderate line pinning due to permalloy bars, and weak random point pinning due to substrate roughness.[11] For details of characteristics of the bubble material and the experimental setup, refer to Ref. 11. The bubble concentration ρ is controlled by a dc magnetic field applied perpendicular to the film plane. The effective temperature is generated by a superimposed ac magnetic field with adjustable peak-to-peak amplitude H_{ac} and fixed frequency 40 Hz. The bubble concentration is adjusted downward by increasing the dc magnetic field in small steps. After each increment of the dc field, the array is annealed at $H_{ac}=20.7$ Oe for 30 min, followed by $H_{ac}=13.6$ Oe for 15 min. The bubbles are directly viewed via Faraday rotation of polarized light in an optical microscope, equipped with a digital-imaging system consist-

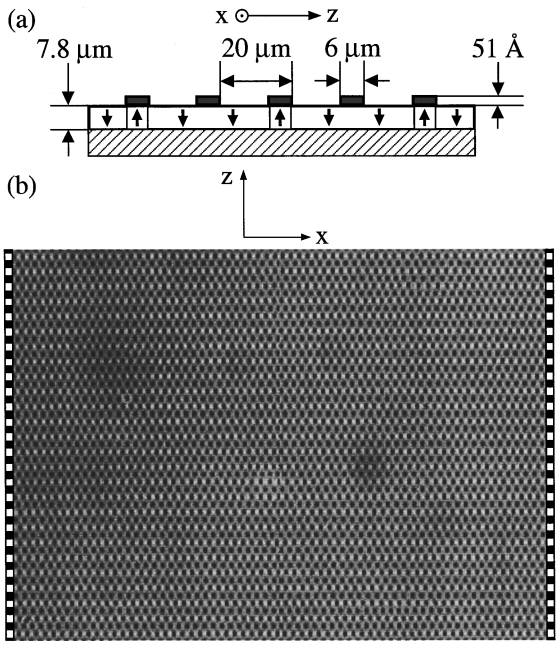

FIG. 1. (a) Schematic cross section of garnet sample: the white layer indicates the garnet with magnetic bubble domains indicated by up arrows; the gray rectangles indicate the cross section of a periodic array of permalloy lines on the film surface, which pin bubbles; the cross hatched layer indicates the substrate. (b) Bubble array image visualized in an optical microscope via Faraday rotation, size 705×517 μm^2. The black squares on the left and right sides represent pinned rows of bubbles; the white squares represent unpinned rows.

ing of a CCD camera, a video cassette recorder, and a Silicon Graphics workstation. Using digital-imaging techniques the locations of bubbles and pinning lines can be easily determined. Figure 1(b) is an image of a commensurately pinned bubble array with every other row of bubbles pinned by the permalloy bars. The locations of the permalloy bars are indicated by the black blocks in the vertical strips on the left and right side of the grayscale image; the white blocks in the bars indicate the locations of the unpinned rows. Periodic parallel pinning produces a hexagonal bubble array with nearest neighbors oriented along the pinning line direction as shown. We choose the x-axis and z-axis directions $\hat{x}$ and $\hat{z}$ parallel and perpendicular to the pinning lines.

III. EXPERIMENTAL RESULTS

Figure 2 is a series of bubble array images processed to show the locations of bubble centers and identify topological defects which illustrates the microscopic nature of array through the commensurate-incommensurate phase transitions. The images are ordered from the highest bubble concentration on the top left to the lowest bubble concentration on the bottom right; only part of the digitized array is shown. Disclinations are identified using Voronoi constructions (see caption). A dislocation is a bound pair of a fivefold and a sevenfold disclination; the Burgers vector is defined to be perpendicular to the line connecting the five-seven pair.

Figures 3(a)–3(i) are plots of the structure functions $S(\mathbf{q})$ corresponding to Figs. 2(a)–2(i), but computed over the

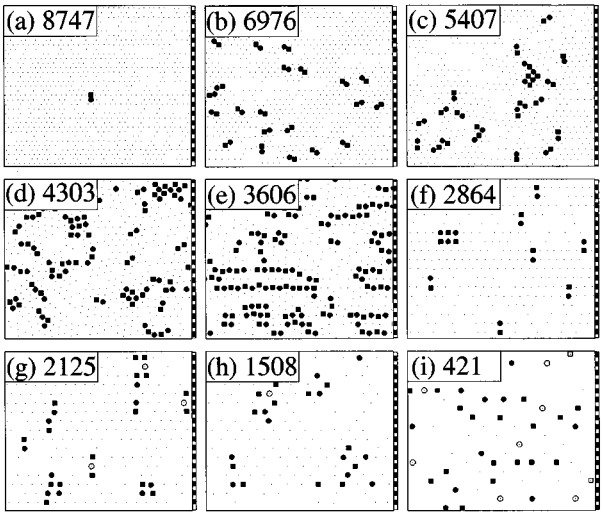

FIG. 2. Overview of commensurate-incommensurate transitions in real space as the bubble concentration ρ is reduced; ρ (mm^{-2}) is indicated on the top left of each 410×351 μm^2 image. The black dots represent bubble centers. Black squares, black circles, open squares, and open circles represent topological defects: fivefold, sevenfold, $<$ fivefold, and $>$ sevenfold disclinations, respectively. A bound fivefold and sevenfold pair of disclinations is a dislocation. The black squares in the right side of each image indicate pinned rows; the white squares unpinned rows.

whole imaging area of 705×517 μm^2. The structure function is defined[12] $S(\mathbf{q})=|\rho(\mathbf{q})|^2$, where $\rho(\mathbf{q})=\Sigma_{j=1}^{N}e^{i\mathbf{q}\cdot\mathbf{r}_j}$ is the Fourier transform of the bubble concentration function with $\mathbf{r}_j$ the positions of bubble centers. A Hanning window with cylindrical symmetry is applied to the bubble center data in

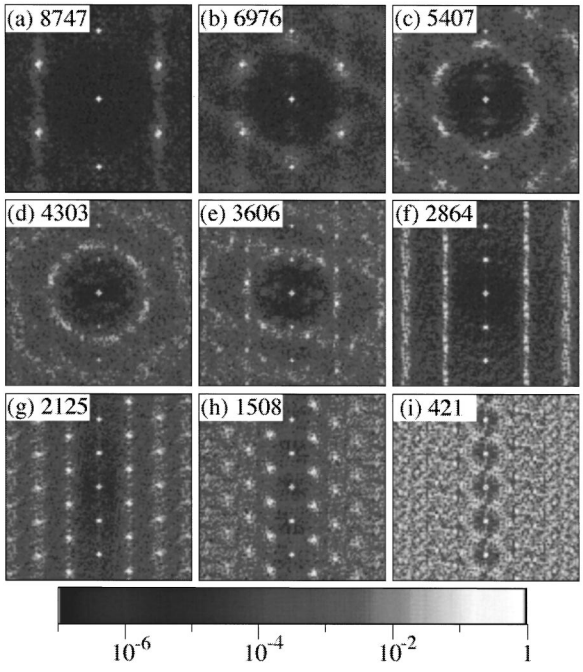

FIG. 3. Structure functions $S(\mathbf{q})$ computed from bubble center locations corresponding to Figs. 2(a)–2(i) (see text) showing commensurate-incommensurate transitions. The origin $q=0$ is at the center of each image; the pinning lines are parallel to the horizontal q_x axis; the q_z axis is vertical.

order to reduce the amplitude of possible spurious features. The average bubble concentrations (bubbles/mm^2) are shown on the top left of each image in Fig. 3, as for Fig. 2.

Using Figs. 2 and 3 together, we can examine the commensurate and incommensurate phases which occur as the bubble concentration is reduced and study the pathway by which the phase transitions take place. We start with the high concentration commensurate phase. Figure 2(a) shows that this phase is a triangular array with the nearest neighbor bond along the pinning line direction $\hat{x}$. The array is commensurate with the pinning line spacing with two rows of bubbles per pinning line. The dislocations are few and far away from each other, with only one present in Fig. 2(a), and all have Burgers vectors in the $\hat{x}$ direction. The corresponding structure factor $S(\mathbf{q})$ in Fig. 3(a) has two peaks at $q_z = \pm 4\pi/s$ that are sharp, indicating a commensurate array. The off-axis peaks are broadened somewhat by point disorder and have Lorentzian shapes. The quasi-long-range orientational order and Lorentzian line shape of off-axis peaks indicate this phase is a dislocated triangular array. Observations of the annealing process in samples with and without line pinning indicate that the pinning acts to stabilize orientational order as one would expect from theory.[3,5]

As the bubble concentration is reduced from $\rho = 8747$ to 7277 mm^{-2}, the array accumulates strain, and the dislocation concentration increases only slightly. The dislocations in this regime are isolated and have horizontal Burgers vectors; this orientation minimizes their interaction with the pinning potential, because the missing rows are not parallel to the pinning lines. A uniaxial strain results from the competition between the pinning potential and reduced concentration:[3] the $\hat{x}$ component q_x of the off-axis peaks in the structure function decreases while the $\hat{z}$ component q_z remains relatively unchanged, and the width of the peaks remains constant.

Figures 2(b)–2(d) and Figs. 3(b)–3(d) show how the array makes the transition from a commensurate triangular array to an incommensurate polycrystalline phase as the bubble concentration is reduced. During annealing, bubbles are seen to move from unpinned rows to neighboring pinned rows, and the average number of bubbles per row in the unpinned rows decreases faster than that in the pinned rows, as one would expect to minimize the energy. As shown in Fig. 2(b) the reduction in bubble concentration is accomplished by the removal of partial rows of unpinned bubbles as indicated by pairs of dislocations with antiparallel Burgers vectors oriented $\pi/3$ radians from the pinning lines. As the bubble concentration is reduced further in Figs. 2(c) and 2(d), the array rotates locally to form a polycrystalline triangular array, and the dislocations group together to form grain boundaries. The structure factor in Fig. 3(b) develops a new diffuse peak located along the z axis with wave vector q_z below the pinning wave vector $4\pi/s$. The wave vector of this diffuse peak decreases with bubble concentration and the peak broadens in the angular direction to form a ring for the polycrystalline array in Fig. 3(d). As shown in Fig. 2(d), this incommensurate polycrystalline phase has substantial disorder. A disordered incommensurate phase has also been observed in monolayer krypton on graphite by Moncton *et al.*[2] using synchrotron x-ray scattering method. We did not observe an incommensurate single crystal, a glass or an incommensurate smectic phase at any of these bubble concentrations.

A commensurate smectic phase forms as the bubble concentration is reduced further as shown in Figs. 2(e) and 2(f). This new phase is characterized by order along $\hat{x}$ but disorder along $\hat{z}$: the bubbles in each pinned row form a periodic one-dimensional array, but the phases of one-dimensional arrays in different rows are not well correlated. Within the smectic phase in Fig. 2(f), the relatively few dislocations present have Burgers vectors oriented parallel to $\hat{x}$. The structure factor of the smectic phase in Fig. 3(f) displays a series of diffuse vertical stripes, together with sharp peaks along the q_z axis with half of the period for Fig. 3(a), corresponding to the periodic pinned rows of bubbles. This smectic phase is different from the one predicted by Balents and Nelson,[5] because the smectic order of the bubble array is along the pinning stripes in the $\hat{x}$ direction, rather than along $\hat{z}$. The experimental result is expected if the pinning potential is stronger than the bubble-bubble interaction for the concentration corresponding to this smectic phase. Other evidence for moderate pinning is that the spacing between bubbles in the same row is shorter than between bubbles in the $\hat{z}$ direction, as shown in Figs. 2(f) and 3(f), and the absence of possible incommensurate single crystal, glass, or incommensurate smectic phases.

A transition from a commensurate smectic to a commensurate triangular array occurs as the bubble concentration is reduced, as shown in Figs. 2(g) and 2(h). In the smectic phase Fig. 2(f), bubbles are compressed in rows along the pinning lines; as the concentration is reduced, the bubble spacing within rows approaches the spacing appropriate for a commensurate triangular array in Fig. 2(g), then exceeds this spacing in Fig. 2(h) as the commensurate array is stretched along the $\hat{x}$ direction. In both Figs. 2(g) and 2(h) the array continues to show disorder in the alignment of pinned rows of bubbles. The structure factor in Fig. 3(g) shows peaks corresponding to the commensurate triangular array with diffuse stripes corresponding to the disorder in row alignment. In Fig. 2(h) the dislocations no longer have a preferred direction, and the disordered background in the structure factor is diffuse. Comparing the commensurately pinned triangular arrays in Figs. 3(h) and 3(a), the low concentration triangular array in Fig. 3(h) possesses twice the bubble spacing and broader off-axis peaks. Finally, as the bubble concentration is reduced further to $\rho = 421$ mm^{-2} in Figs. 2(i) and 3(i) the array melts into a modulated liquid: the dislocations unbind into isolated disclinations as shown in Fig. 2(i), and the structure function Fig. 3(i) is a superposition of a diffuse background with sharp peaks at $q_z = \pm 2\pi/s$ and $\pm 4\pi/s$ along $\hat{z}$, due to the pinning potential.

The phase transition between the high concentration commensurate triangular array in Fig. 3(a) and the commensurate smectic phase in Fig. 3(f) is second order (or weakly first order), as demonstrated by the formation and smooth migration of a diffuse peak in the structure factor along $\hat{z}$. Figure 4 plots the position of the diffuse peak vs bubble concentration, along with error bars indicating the full width at half maximum. Two diffuse peaks appear along the q_z axis in Figs. 3(b) when the bubble concentration becomes incommensurate. The positions of these peaks shift smoothly from $q_z = \pm 4\pi/s$ to $q_z = \pm 2\pi/s$ as the concentration is reduced,

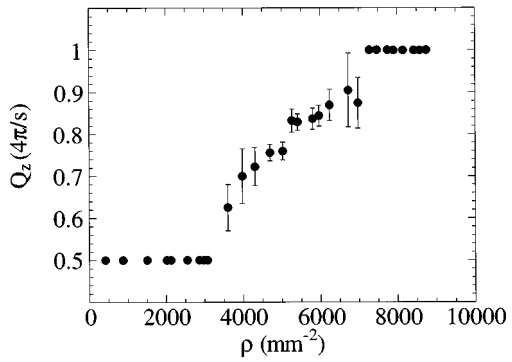

FIG. 4. Smooth migration of the wave vector Q_z of the diffuse peak vs bubble concentration ρ. The error bars represent the full width at half maximum.

as shown in Fig. 4. Above $\rho=7000$ mm^{-2} and below $\rho=3500$ mm^{-2} the diffuse peak is absent and the array is commensurate. These data affirm that the commensurate triangular array to commensurate smectic transition takes place via the formation of a polycrystalline array in which the array is locally rotated with incommensurate bubble spacing as discussed above. The smooth migration of the Bragg peaks agrees with theoretical predictions for krypton on graphite and layered superconductor systems.[1,5] If one looks carefully at Fig. 3, one also finds the appearance of two peaks along $\hat{z}$ at wave vector $q_z=\pm 2\pi/s$, half the value for the initial high concentration commensurate phase. These peaks arise from the period of the pinning potential rather than from any first order transition and are absent in Fig. 3(a) only because they are forbidden by the symmetry of the high concentration commensurate phase.[13]

ACKNOWLEDGMENTS

We thank R. Belt of Litton Industries for providing garnet samples. The authors especially thank D. R. Nelson and L. Balents for suggestion of the line pinning experiment and many constructive discussions. We also benefited from discussion with E. Frey. This work is supported in part by NSF Grant No. DMR-94-00396 and ONR Contract No. N00014-95-1-0104.

[1] S. N. Coppersmith, D. S. Fisher, B. I. Halperin, P. A. Lee, and W. F. Brinkman, Phys. Rev. Lett. **46**, 549 (1981); Phys. Rev. B **25**, 349 (1982); V. L. Pokrovsky and A. L. Talapov, Phys. Rev. Lett. **42**, 65 (1979).

[2] P. M. Horn, R. J. Birgeneau, P. Heiney, and E. M. Hammonds, Phys. Rev. Lett. **41**, 461 (1978); D. E. Moncton, P. W. Stephens, R. J. Birgeneau, P. M. Horn, and G. S. Brown, *ibid.* **46**, 1533 (1981).

[3] S. E. Burkov and V. L. Pokrovsky, J. Low Temp. Phys. **44**, 423 (1981); JETP Lett. **32**, 263 (1981).

[4] O. Daldini, P. Martinoli, J. L. Olsen, and G. Berner, Phys. Rev. Lett. **32**, 218 (1974); P. Martinoli, H. Beck, M. Nsabimana, and G.-A. Racine, Physica B **107**, 455 (1981).

[5] L. Balents and D. R. Nelson, Phys. Rev. Lett. **73**, 2618 (1994); Phys. Rev. B **52**, 12 951 (1995).

[6] B. I. Ivlev and N. B. Kopnin, J. Low Temp. Phys. **80**, 161 (1990); B. I. Ivlev, N. B. Kopnin, and V. L. Pokrovsky, *ibid.* **80**, 187 (1990); L. S. Levitov, Phys. Rev. Lett. **66**, 224 (1991).

[7] R. Seshadri and R. M. Westervelt, Phys. Rev. Lett. **70**, 234 (1993); Phys. Rev. B **47**, 8620 (1993).

[8] D. R. Nelson and B. I. Halperin, Phys. Rev. B **19**, 2457 (1979).

[9] R. Seshadri and R. M. Westervelt, Phys. Rev. Lett. **66**, 2774 (1991); D. G. Grier *et al.*, *ibid.* **66**, 2270 (1991).

[10] Y. Imry and S. Ma, Phys. Rev. Lett. **35**, 1399 (1975).

[11] Junmin Hu and R. M. Westervelt, Phys. Rev. B **51**, 17 279 (1995).

[12] D. R. Nelson, M. Rubinstein, and F. Spaepen, Philos. Mag. A **46**, 105 (1982).

[13] D. R. Nelson (private communication).